Potential energy and dipole moment surfaces of H-3(-) molecule

M. Ayouz

R. Guérout

J. Robert

V. Kokoouline
University of Central Florida

Recommended Citation

University of
Central
Florida

STARS
Showcase of Text, Archives, Research & Scholarship

M. Ayouz, O. Dulieu, R. Guérout, J. Robert, and V. Kokoouline

ARTICLES YOU MAY BE INTERESTED IN

The Structure of H₃, H₃⁺, and of H₃⁻. IV
The Journal of Chemical Physics **5**, 933 (1937); https://doi.org/10.1063/1.1749966

Potential Energy Surface for H₃
The Journal of Chemical Physics **40**, 1105 (1964); https://doi.org/10.1063/1.1725256

Potential energy and dipole moment surfaces of HCO⁻ for the search of H⁻ in the interstellar medium
The Journal of Chemical Physics **136**, 224310 (2012); https://doi.org/10.1063/1.4724096

Potential energy and dipole moment surfaces of H₃⁻ molecule

M. Ayouz,[1] O. Dulieu,[1] R. Guérout,[1] J. Robert,[1] and V. Kokoouline[1,2,a)]
[1]*Laboratoire Aimé Cotton, CNRS, Bât. 505, Université Paris-Sud, 91405 Orsay Cedex, France*
[2]*Department of Physics, University of Central Florida, Orlando, Florida 32816, USA*

A new potential energy surface for the electronic ground state of the simplest triatomic anion H₃⁻ is determined for a large number of geometries. Its accuracy is improved at short and large distances compared to previous studies. The permanent dipole moment surface of the state is also computed for the first time. Nine vibrational levels of H₃⁻ and 14 levels of D₃⁻ are obtained, bound by at most $\sim$70 and $\sim$126 cm⁻¹, respectively. These results should guide the spectroscopic search of the H₃⁻ ion in cold gases (below 100K) of molecular hydrogen in the presence of H⁻ ions. © *2010 American Institute of Physics*. [doi:10.1063/1.3424847]

I. INTRODUCTION

Collisions involving hydrogen atoms, molecules, and their positive (H^+, H_2^+) and negative (H^-) ions play an important role in chemistry and evolution of neutral or negatively charged hydrogen plasma such as laboratory hydrogen plasma, the interstellar medium (ISM), atmospheres of the Sun and other stars,[1] as well as the Earth atmosphere. Binary collisions of these species are simple enough to be treated using first principle methods without any adjustable parameter. Therefore, such processes are often used as benchmarks for testing theoretical methods.

The existence of bound states of the H₃⁻ ion in a linear configuration for the three nuclei has been suggested in 1937,[2] but has been questioned since then. Different *ab initio* calculations[3–11] have been giving contradictory results for the depth of the potential well. The estimated error bar in the calculations was comparable or larger than obtained binding energies, so the calculations could not predict for sure if the H₃⁻ ion is stable. Although first observations of H₃⁻ ions have been reported in low resolution experiments as early as in 1974,[12–17] they could not warrant either the stability of H₃⁻. It is only in the 1990s (Refs. 10 and 18) that theory became precise enough to confirm the stability of the H₃⁻ anion.

At present, there are three available accurate potential energy surfaces (PES) of H₃⁻: the PES by Stärck and Meyer,[10] by Belyaev and Tiukanov,[19] and by Panda and Sathyamurthy.[11] In the following, these three PES will be referred to as PES-SM, PES-BT, and PES-PS, respectively. In addition, Belyaev *et al.*[19–24] have obtained PES of excited electronic states of H₃⁻ and their non-Born–Oppenheimer[25] couplings with the ground state. The excited electronic states are unstable with respect to electron autodetachment. Bound state calculation based on the PES-SM have been performed for H₃⁻, H₂D⁻, and D₂H⁻ in Ref. 10 and using the PES-BT for H₃⁻ in Ref. 16. It is worth to mention a stand alone study by Robicheaux[18] confirming the stability of H₃⁻ (and similar an-

ions), where the PES was derived from the scattering length for the electron-H₂ collisions, and from the polarizability of H₂.

While never observed in the ISM, the collisions between H₂ and H⁻, and of their isopotologues, have been studied in a number of laboratory experiments back to the 1950s.[26–32] Such collisions should also play a role in processes in tokamaks, especially if the negative ion source (D⁻) is used for the tokamak neutral beam injectors.[33,34] Many studies have been devoted to the calculation of elastic and inelastic cross sections for H_2-H^- collisions and for all isopotologues,[11,24,35–46] most of them for energies significantly larger than 1 eV above the lowest dissociation limit of H_2+H^-. However, at such energies the theoretical cross sections may not be reliable. The dissociation energy of the H₃ ground state lies only 0.75 eV above the H₃⁻ dissociation energy, and the non-Born–Oppenheimer interaction between the ground states of H₃ and H₃⁻ could be significant. The non-Born–Oppenheimer interactions have been taken into account only in Ref. 47 within a reduced-dimensionality approach, where only linear geometries of H₃⁻ have been taken into account. Finally, the photodissociation of H_2D^- has been studied in a simplified approach based on the Franck–Condon overlap between a bound level and a scattering state of H_2D^-,[48] since the *ab initio* dipole moments of H₃⁻ were not available at that time.

The present study is mainly motivated by the formation of H₃⁻ bound states in low-energy collisions between H₂ and H⁻. In such collisions H₃⁻ can be formed only if a third body (other than H₂ or H⁻) participates (three-body recombination) or if a photon is emitted [radiative association (RA)]. Both processes could be relevant for the chemistry of cold interstellar clouds, if H⁻ is present.[49] Note that the H⁻ ion has not been detected so far in the ISM: it cannot be directly observed by usual photoabsorption spectroscopy because H⁻ has only one bound electronic state.

The evaluation of the cross section for RA of H₂ and H⁻ at low energy (10–30 K) requires an accurate PES with a precision around 1 cm⁻¹ or better, and permanent dipole moment surfaces (PDMS) for H₃⁻. In the present study, we calculated a new *ab initio* PES for the H₃⁻ electronic ground

a)Electronic mail: slavako@mail.ucf.edu.

state on a dense and large grid for internal coordinates, using a larger electronic basis set than those of PES-SM and PES-PS calculations. Special care is taken in order to account for the long-range behavior of the surface. We also obtain for the first time the PDMS of the H_3^- electronic ground state. We constructed FORTRAN subroutines, yielded as supplementary material to the paper, that calculate PES and PDMS values for any arbitrary geometry using B-spline interpolation procedures, and we determine the bound states of H_3^- and D_3^-. The RA reaction will be treated in a separate study.

The article is organized in the following way. In Sec. II, we discuss the calculation of the new PES and the interpolation procedure. In Sec. III, we compare the new PES with the PES from previous studies. Section IV is devoted to the calculation of bound levels of H_3^- and D_3^- and Sec. V presents our results on the dipole moment of H_3^-. Section VI is the conclusion. Atomic units (a.u.) for distances (1 a.u. =0.052 917 7 nm) and for energies (1 a.u. =219 474.631 37 cm^{-1}) will be used throughout the paper, except otherwise stated.

II. *AB INITIO* CALCULATION AND INTERPOLATION OF THE H_3^- GROUND STATE POTENTIAL SURFACE

As in Ref. 10, we used the coupled-electron pair approximation (CEPA-2) method,[50] which is part of the MOLPRO package.[51] It is a nonvariational variant of the configuration interaction method for closed-shell molecules. Here we used a considerably larger basis set, AV5Z with *spdfg* basis functions from the MOLPRO basis library, and a much larger number of geometries, than in Refs 10 and 11. The reasons for choosing this method and a comparison with other *ab initio* methods are presented in Appendix, Sec. 1.

As explained below, the H_3^- molecule is weakly bound by long-range electrostatic forces with no electron exchange. We defined a three-dimensional (3D)-grid in Jacobi coordinates: r—the distance between two protons, R—the distance from the center of mass of the two protons to the third proton, and γ—the angle between vectors $\vec{R}$ and $\vec{r}$. The grid in r is uniform from $r=0.8$ a.u. to $r=2.4$ a.u. and changes by a step $\Delta r=0.2$ a.u. The grid in γ changes from 0° to 90° by a constant step of $\Delta\gamma=15°$. The grid in R was chosen denser for small R than for large R: the grid points R_i were calculated according to $R_i=1.5+0.452\exp(i/10)$ (in a.u.) with $i=1,2,\cdots,48$, which makes R changing from 1.9995 to 56.4227 a.u. Therefore, the calculations were performed for $9\times7\times48=3024$ geometries. Notice that the above grid starts at a smaller value of $r=0.8$ a.u. than in Refs. 10 and 11 ($r=1$ a.u.). Indeed, we found that a grid starting at $r=1$ a.u. cannot properly represent the repulsive part of the H_2 ground state potential curve (at fixed R and γ) and gives an appreciable error in energies obtained of the lowest H_2 vibrational levels and, as a result, a comparable error in dissociation
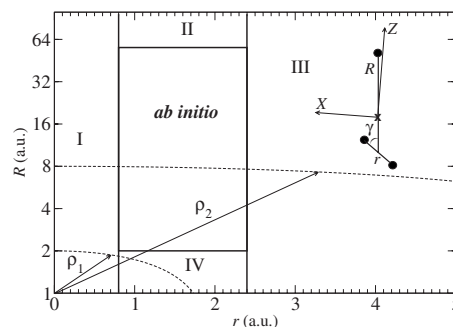

FIG. 1. The five regions of the configuration space in Jacobi coordinates R,r defined for the PES calculations, for all values of γ (see the text). Notice that R is given on a logarithmic scale. The central rectangle represents the region of calculated *ab initio* points, where a 3D B-spline interpolation is used. Different methods were used for the extrapolation of the PES and PDMS in regions I-IV (see text). The arcs of a circle (dashed lines) represent lines of fixed hyper-radii ρ (see Sec. IV) for two values, ρ_1 =2 a.u. and ρ_2=8 a.u. The X, Y, and Z axes (needed to specify the components of the PDM vector) are the axes of principal moments of inertia. Their orientation is indicated in the figure. The Y-axis is out the plane of H_3^-.

energies of $H_3^-\rightarrow H_2(v,j)+H^-$ when $R\rightarrow\infty$. We also used a denser grid in γ and a longer and denser grid in R than in Refs. 10 and 11.

For each geometry, we calculated the potential energy of the H_3^- ground state, and the components of the PDM vector with respect to the principal axes of inertia. The obtained *ab initio* PES and PDMS were used to prepare FORTRAN subroutines that calculate PES and PDMS for any arbitrary geometry. The FORTRAN subroutines are available in the supplementary material[72] and can be provided by the authors upon request. Inside the 3D box $r\in[0.8;2.4]$, $R\in[1.9995;56.4227]$, $\gamma\in[0;360°]$ (central region in Fig. 1) the procedures interpolate the surfaces using the 3D B-spline method. Outside of the box, the procedures rely on analytical formulas for the extrapolation of PES and PDMS. To simplify the description of this region, we divided the $r\times R$ configuration space in four different parts (I-IV) surrounding the *ab initio* rectangle (Fig. 1). Regions "*ab initio*" and II are the only ones relevant to bound and scattering states of the system with energies $\lesssim2$ eV above the $H_2(v=0,j=0)+H^-$ dissociation. Therefore, the extrapolation procedure for the PES and PDMS in the two regions should be physically justified. In contrast, wave functions of bound and continuum states with such energies vanish in regions I, III, and IV, and empirical formulas will be used. As it will be discussed in Sec. IV, the extrapolation is needed to map the configuration space in Jacobi coordinates on the space of hyperspherical coordinates, which will be used for bound state and scattering calculations.

In region II, we represent the long-range (in R, at fixed r and γ) potential V_{LR} for the interaction between H_2 and H^- as[52]

$$V_{LR}(R;r,\gamma)=D_{as}(r)+\frac{C_3^{th}}{R^3}+\frac{C_4^{th}}{R^4},$$

with

$$C_3^{th} = -Q(r)P_2(\cos\gamma) \quad \text{and}$$

$$C_4^{th} = -[\alpha_0(r) + \alpha_2(r)P_2(\cos\gamma)]/2, \tag{1}$$

where the first term $D_{as}(r)$ is the sum of H^- and H_2 energies at a given internuclear distance r of the H_2 molecule. The second term is the interaction between the electric charge of H^- with the quadrupole moment $Q(r)$ of H_2 (taken from Ref. 53), and the third term is the interaction of the dipole moment of H_2 induced by H^-, involving the second order Legendre polynomial $P_2(\cos\gamma)$. The functions $\alpha_0(r)$ and $\alpha_2(r)$ are the isotropic and anisotropic polarizabilities of H_2, for which we used the analytical functions given in Ref. 11 that were obtained by fitting the numerical values from Ref. 54. The dispersion energy varying as $1/R^6$ and other smaller terms are neglected, which is a good approximation because the long-range expansion is only used for $R > 56.4$ a.u. Notice that the leading term is attractive for $\gamma=0°$ and repulsive for $\gamma=90°$.

In region I we used the following extrapolation formula in r for fixed R and γ:

$$V_{SR}(r;R,\gamma) = a(R,\gamma)e^{-b(R,\gamma)r}, \tag{2}$$

where $a(R,\gamma)$ and $b(R,\gamma)$ are functions of R and γ that are obtained considering the two *ab initio* energies $V(r=0.8;R,\gamma)$ and $V(r=1;R,\gamma)$ calculated at the first two values of the coordinate r. In this way, we obtain the quantities a and b given on a two-dimensional (2D) grid of points in the (R,γ) space. Then we used the 2D B-spline interpolation to obtain smooth 2D functions $a(R,\gamma)$ and $b(R,\gamma)$.

In region III, we extrapolate the PES in r and at fixed R and γ using a dispersion-like expression

$$V_{LR}(r;R,\gamma) = D_0(R,\gamma) - \frac{C_6(R,\gamma)}{r^6}, \tag{3}$$

where the $D_0(R,\gamma)$ and $C_6(R,\gamma)$ (always positive) coefficients are obtained in a way similar to the coefficients a and b, considering the two last points $V(r=2.2 \text{ a.u.};R,\gamma)$ and $V(r=2.4 \text{ a.u.};R,\gamma)$. They are also interpolated using the 2D B-spline method for arbitrary values of R and γ.

The behavior of the PES in region IV is described by the short-range (in R) repulsive expression at given values of r and γ

$$V_{SR}(R;r,\gamma) = A(r,\gamma)e^{-B(r,\gamma)R}. \tag{4}$$

The $A(r,\gamma)$ and $B(r,\gamma)$ coefficients are obtained in a way similar to the one described above, considering the first two values of the *ab initio* potential energy $V(R=2 \text{ a.u.};r,\gamma)$ and $V(R=2.052 \text{ a.u.};r,\gamma)$, and are further interpolated for any (r,γ) using the same 2D B-spline procedure.

We show in Fig. 2 the H_3^- PES as a function of two internuclear distances, r_1 and r_2 for two values (180° and 90°) of the bonding angle δ. These coordinates are convenient to describe main features of the PES. As expected, the figure is symmetric with respect to the $r_1 \leftrightarrow r_2$ exchange, and shows the shallow potential well in each coordinate (with the minimum labeled with M), separated by a potential barrier (with the maximum labeled with B) for the exchange of two
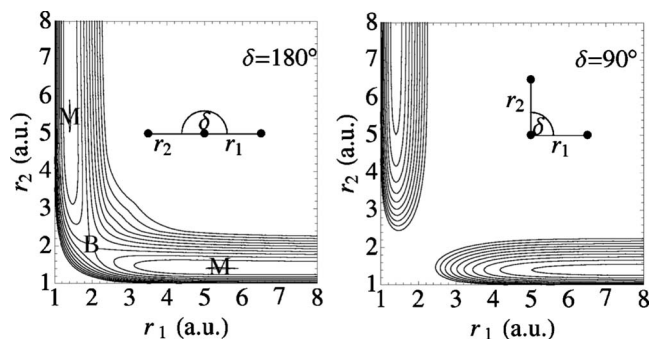

FIG. 2. Energy contour plots of the H_3^- electronic ground state PES in the space of the two internuclear distances (r_1 and r_2) for two values of the bonding angle δ defined in each plot. Successive contours differ by 0.006 a.u. The dissociation energy $D_{as} = -1.701\ 682\ 8$ a.u. of the PES corresponds to the infinite separation between $H_2(r_e=1.403$ a.u.$)$ and H^- (see Table I). The energy minimum (indicated by M) is obtained for a linear configuration, and the top of the potential barrier is labeled with B. The lowest contour corresponds to the energy of -1.7034 a.u. (left plot) and -1.6974 a.u. (right plot).

identical nuclei. As in previous studies, the lowest energy is found for a linear configuration as expected from Eq. (1). The position and energy of M and B are reported in Table I, together with other characteristic parameters of the PES.

III. COMPARISON WITH PREVIOUS STUDIES

Figures 3–5 illustrate the comparison of the PES in Jacobi coordinates obtained in the present study with the results of Refs. 10 and 11 for three values of $\gamma=0°$, 30°, and 90°, respectively. Each figure gives the PES for one value of γ and eight values of r versus the coordinate R. The origin of potential energy yielded by the *ab initio* procedure corresponds to an infinite separation of all electrons and nuclei. Because the absolute energy of the PES-PS (Ref. 11) is unknown, the origin of this surface is chosen in such a way that the asymptotic energy of the infinite separation between $H_2(r=1.4$ a.u.$)$ and H^- is the same as in the present study. We would like to stress that the present CEPA-2 method gives the energy of H_3^- at $R\to\infty$ exactly equal to the sum of H_2 and H^- energies calculated separately within the same approach (Table I). Moreover, the asymptotic energy is remarkably accurate: the hydrogen electronic affinity is obtained at 6019.97 cm^{-1}, in good agreement with experimental value 6082.96 cm^{-1}.[56] Similarly, our electronic binding energy of H_2, $E_{H_2(r_e)} = -1.174\ 252$ at its equilibrium distance $r_e=1.4$ only differs by 49 cm^{-1} from the almost exact Born–Oppenheimer energy computed by Wolniewicz and Dressler.[55] These results confirm the good accuracy of the total energy obtained with the CEPA-2 method.

The insets of these figures, together with the data in Table I demonstrate that the present *ab initio* energies are systematically lower that those of Ref. 10 for all geometries. For instance, the potential well depth has increased by 0.01% (around 160 cm^{-1}) at $r_e=1.4$ a.u. This was expected, as we use the same CEPA-2 method than in Ref. 10 with a larger basis set, leading then to a PES with an improved accuracy. The overall behavior of the present PES and PES-SM as a function of R is similar at small and large distances. In contrast, a noticeable difference of PES-PS with the present re-

TABLE I. Different quantities characterizing the H_3^- ground state PES obtained in the present study compared with previous calculations (Refs. 10, 11, and 19).

Quantity	Present study	Ref. 10	Ref. 11	Ref. 19
D_{as}[a] (a.u.)	−1.701 683	−1.700 95	n/a	n/a
r_e[b] (a.u.)	1.403	1.40	n/a	n/a
B[c] (a.u.)	−1.685 09	−1.685 62	n/a	n/a[d]
Position of B				
r_1, r_2 (a.u.), $\delta=0$	1.996, 1.996	1.997, 1.997	1.999, 1.999	1.74, 1.74
r, R (a.u.), $\gamma=0$	1.996, 2.994	1.997, 2.996	1.999, 2.999	1.74, 2.61
M[e] (a.u.)	−1.703 511	−1.702 70	n/a	n/a
Position of M				
r, R (a.u.), $\gamma=0$	1.421, 6.069	1.416, 6.183	1.419, 5.915	n/a
$B-M$ (cm^{-1})	4042.9	3748.62	3786.42	n/a
$D_{as}-M$ (cm^{-1})	401.2	384.05	384.27	443.60
	Energies obtained separately for H_2 and H^-			
	Present study	Ref. 10	Ref. 55	Ref. 56
$E_{H_2(r=1.4)}$	−1.174 252	−1.173 68	−1.174 475 7	n/a
E_{H^-}	−0.527 429	−0.527 27	n/a	0.527 716[f]

[a]Asymptotic energy at infinite separation between $H_2(r_e)$ and H^-.
[b]Internuclear distance corresponding to the minimum of the H_2 dimer potential.
[c]Energy of the maximum of the barrier, B in Fig. 2.
[d]Reference 19 gives the height of the barrier (0.624 eV) with respect to the $H_2(v=0, j=0)+H^-$ dissociation.
[e]Energy of the PES minimum, M in Fig. 2.
[f]Energy is obtained by adding 0.5 a.u. to the experimental affinity (Ref. 56) of H^-.

sults and the PES-SM is the presence of a potential well at $\gamma=90°$ near $R=7.6$ a.u. (see the inset in Fig. 5) with a significant depth (~ 90 cm^{-1} for $r=1.4$ a.u.). For $\gamma=90°$ the C_3/R^3 long-range energy contribution is positive and C_4/R^4
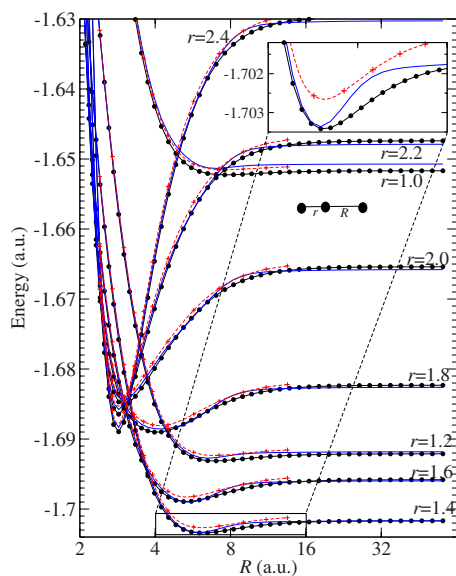

FIG. 3. Comparison of the present H_3^- PES (circles) in Jacobi coordinates with the results from Ref. 10 (crosses on the dashed lines) and Ref. 11 (solid blue lines with no symbols) for $\gamma=0°$. The PES are shown as a function of R for eight different values of r. The $r=0.8$ a.u. curve is not shown here because it is located at a higher energy. Symbols indicate the geometries for which the actual *ab initio* calculations have been performed. The continuous lines connecting the points are obtained by interpolation. No *ab initio* energies are available for the PES of Ref. 11. The solid lines without symbols are obtained directly from the analytic formula and the FORTRAN subroutine provided in Ref. 11. Notice the logarithmic scale in R variable. The inset enlarges the region of the minimum of the PES close to equilibrium region at $r=1.4$ a.u.
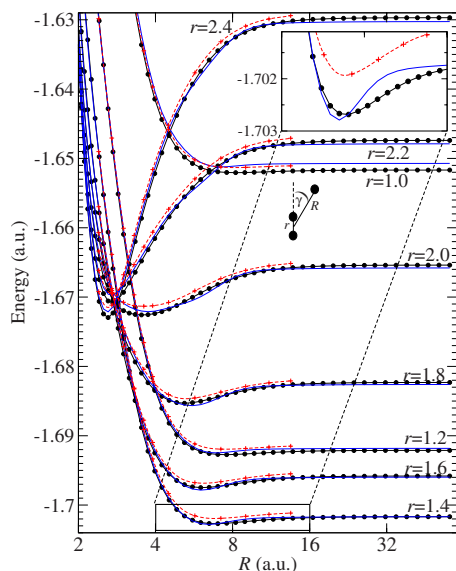
is negative [see Eq. (1)]. Therefore, their sum combined with the short-range interaction produces a potential curve (for fixed r and γ near 90°) that has a pronounced minimum in PES-PS and just a shoulder-like feature in the present PES [see inset (c) in Fig. 5]. The curve is repulsive asymptotically. A possible reason for the above differences is the somewhat smaller basis set (d-aug-cc-PVTZ) used in calculation of PES-PS.[11]

The numerical data available about PES-BT[19,23] is given in Table I. Since the calculation method (diatomics-in-molecule) explicitly uses the *ab initio* data (wave functions and energies) obtained for fragments (H_2, H^-, H_2^-, H_3) in separate *ab initio* calculations, it gives automatically the correct dissociation energy.

Since we have calculated PES at relatively large distances R, we can extract *ab initio* values (labeled with "ai") of the corresponding long-range coefficients C_3^{ai} and C_4^{ai} and compare them with the theoretical values C_3^{th} and C_4^{th} of Eq. (1). We first make a fit of C_4^{ai} to the *ab initio* data by fixing C_3^{ai} to the theoretical value C_3^{th}. In this way the value of C_4^{ai} agrees with the value of C_4^{th} within 0.3% for $\gamma=0$, and 5% for $\gamma=90°$ at $r=1.4$ a.u. Then, we did the opposite: we fitted C_3^{ai} to the *ab initio* data by fixing C_4^{ai} to C_4^{th}. In this case, we found that fitted and theoretical values of C_3 agree within 0.1% for $\gamma=0$ and 2% for $\gamma=90°$ at $r=1.4$ a.u. The PES-PS differs significantly from the analytical long-range behavior of Eq. (1). Surprisingly, the long-range behavior of the PES-PS is quite different from ours and the one of PES-SM, and probably inaccurate due to the matching procedure between the long and short distances used by these authors.

IV. VIBRATIONAL STATES OF H_3^- AND D_3^-

As mentioned in the introduction, one of the motivations of this study is to describe low-energy collisions between H_2

FIG. 4. Same as Fig. 3 except $\gamma = 30°$.

FIG. 5. Same as Fig. 3 except $\gamma = 90°$. The two insets [(b) and (c)] show the behavior of the potentials for $r = 1.4$ a.u. on two different enlarged scales. Region (b) is the enlarged version of (a) and region (c) is enlarged (b).

and H$^-$, and to investigate the formation of H$_3^-$ in such collisions. Therefore, we need an approach which treats both bound and continuum states of the triatomic anion (including rearrangement of nuclei). We use the Smith–Whitten hyperspherical coordinates:[57] a hyper-radius ρ and two hyperangles θ, ϕ, which can be defined for the three identical particles by the three internuclear distances $r_i, (i=1,2,3)$ as
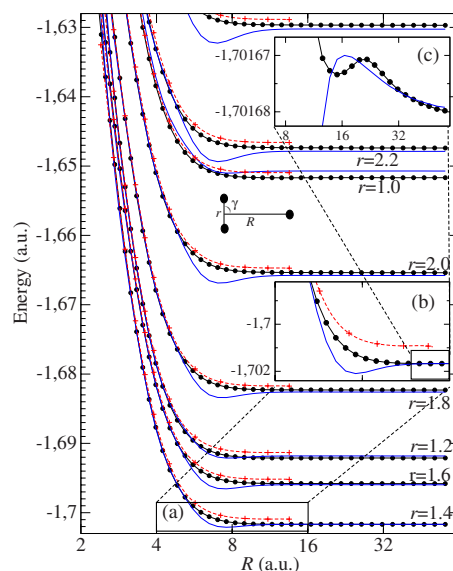
$$r_i = 3^{-1/4}\rho\sqrt{1 + \sin\theta\sin(\phi + \epsilon_i)}, \qquad (5)$$

where $\epsilon_1 = 2\pi/3$, $\epsilon_2 = -2\pi/3$, and $\epsilon_3 = 0$. We also employ the adiabatic separation between hyper-radius and hyperangles, which are known to be well adapted to atom-molecule inelastic and reactive scattering involving identical particles. The dynamics is treated within the framework of the slow variable discretization (SVD) method[58–60] that allows us to account easily for nonadiabatic couplings[25] between hyperspherical adiabatic channels. We briefly recall below the main steps of our approach, which is discussed in greater details in Refs. 59 and 60.

The eigenstates Ψ of three particles interacting through a potential V depending only on the three internuclear distances are obtained by solving the Schrödinger equation with the following Hamiltonian expressed in hyperspherical coordinates ρ, ω in the center-of-mass frame:[57]

$$-\frac{1}{2\mu}\rho^{-5}\frac{\partial}{\partial\rho}\rho^5\frac{\partial}{\partial\rho} + \frac{\Lambda^2}{2\mu\rho^2} + V, \qquad (6)$$

where $\mu = m/\sqrt{3}$ is the three-body reduced mass and m is the mass of each of the three identical particles. The operator Λ above is the grand angular momentum.[61,62] It depends only on the set ω of five angles, which include the three Euler angles (for the orientation of the molecular frame in the laboratory frame) and the hyperangles θ and ϕ. If the total angular momentum $J = 0$, Λ depends only on the two hyperangles. The explicit form of Λ^2 is given, for example, by Eq. (27) of Ref. 62

$$\Lambda^2 = -\frac{4}{\sin(2\theta)}\frac{\partial}{\partial\theta}\sin(2\theta)\frac{\partial}{\partial\theta} - \frac{4}{\sin^2(\theta)}\frac{\partial^2}{\partial\phi^2} + \frac{2J_X^2}{1 - \sin\theta}$$
$$+ \frac{2J_Z^2}{1 + \sin\theta} + \frac{J_Y^2}{\sin^2\theta} + \frac{4i\cos\theta J_Y}{\sin^2\theta}\frac{\partial}{\partial\phi}, \qquad (7)$$

where J_X, J_Y, and J_Z are the components of the angular momentum along the principal axes of inertia. The orientation of the axes is approximately indicated in Fig. 1. After rescaling the wave function Ψ as $\Psi = \rho^{-5/2}\psi$, the Hamiltonian for the new function ψ is written as

$$H = T_\rho + H_{ad}, \qquad (8)$$

where

$$T_\rho = -\frac{1}{2\mu}\frac{\partial^2}{\partial\rho^2}, \qquad (9)$$

and

$$H_{ad} = \frac{\Lambda^2 + 15/4}{2\mu\rho^2} + V. \qquad (10)$$

The eigenfunctions $\psi(\rho, \omega)$ of the above Hamiltonian are sought as an expansion over the basis functions $y_{a,j}(\rho, \omega)$ with unknown coefficients $c_{a,j}$

$$\psi(\rho, \omega) = \sum_{a,j} y_{a,j}(\rho, \omega)c_{a,j}. \qquad (11)$$

The basis functions $y_{a,j}(\rho, \omega)$ are constructed as products

$$y_{a,j}(\rho, \omega) = \pi_j(\rho)\varphi_{a,j}(\omega), \qquad (12)$$

where the functions $\pi_j(\rho)$ are discrete variable representation (DVR)-like functions localized at DVR grid points ρ_j along the hyper-radius. As in our earlier study,[63,64] here we used the plane wave DVR functions. The functions $\varphi_{a,j}(\omega)$ are the adiabatic hyperspherical states obtained by solving the three-body Schrödinger equation at fixed $\rho = \rho_j$, i.e., they are eigenstates of H_{ad} at fixed $\rho = \rho_j$ with eigenvalues $U_a(\rho_j)$

$$H_{\mathrm{ad}}^{\rho=\rho_j}\varphi_{a,j}(\omega) = U_a(\rho_j)\varphi_{a,j}(\omega). \qquad (13)$$

The functions $U_a(\rho_j)$ are usually referred to as hyperspherical adiabatic potentials. Inserting the expansion of Eq. (11) into the Schrödinger equation $H\psi = E\psi$ reduces the equation to a generalized eigenvalue problem for coefficients $c_{a,j}$ with eigenvalues E

$$\sum_{a'j'}\left[\langle\pi_{j'}|-\frac{1}{2\mu}\frac{\partial^2}{\partial\rho^2}|\pi_j\rangle_\rho O_{a'j',aj} + \langle\pi_{j'}|U_a(\rho)|\pi_j\rangle_\rho\delta_{a'a}\right]c_{j'a'}$$

$$= E\sum_{a'j'}\langle\pi_{j'}|\pi_j\rangle_\rho O_{a'j',aj}c_{j'a'}, \qquad (14)$$

where $O_{a'j',aj}$ are the overlap integrals (in the ω space) between adiabatic states $\varphi_{a',j'}$ and $\varphi_{a,j}$

$$O_{a'j',aj} = \langle\varphi_{a',j'}|\varphi_{a,j}\rangle_\omega. \qquad (15)$$

The subscripts ρ and ω at kets in the above expressions refer to the integration coordinate of the bracket.

The system (14) of equations resembles to the system of coupled-channel equations, where nonadiabatic couplings

$$\langle\varphi_{a'}|\frac{\partial}{\partial\rho}|\varphi_a\rangle\frac{d}{d\rho}$$

and

$$\langle\varphi_{a'}|\frac{\partial^2}{\partial\rho^2}|\varphi_a\rangle,$$

are replaced with the overlap matrix elements $O_{a'j',aj}$. The use of overlap matrix elements instead of the derivatives of adiabatic states with respect to ρ simplifies significantly the numerical solution of the equation,[59,60] and is the main advantage of the SVD method.

We restricted the present computations to energies and wave functions of bound states for two H_3^- and D_3^-, with total angular momentum $J=0$. The hyperangle θ varies in the interval $[0,\pi/2]$, while the full interval of variation for the second hyperangle, ϕ, is $[0,2\pi]$. However, for three identical particles, the interval along ϕ can be restricted to $[-\pi/2,-\pi/6]$ for wave functions of the A_1' or A_2' irreducible representations (*irreps* in the following) of the molecular symmetry group (D_{3h}), and to the interval $[-\pi/2,+\pi/2]$ for wave functions of the E' irrep. Irreps with odd parities, A_1'', A_2'', and E'' are not allowed for $J=0$. This is because the inversion applied to the rotational part of the total wave function is reduced to the rotation of the system about the Y-axis by π.[65] The $J=0$ rotational states are isotropic, so only the even parity is allowed. The hyper-radius ρ can vary in the interval $[0,\infty)$. In this study, it varies from 1 to 120 a.u. for H_3^- a.u. and from 1 to 80 a.u. for D_3^-. In the numerical calculation, we have used equal masses $m = 1837.3621$ a.u. for all three atoms in the H_3^- molecule. This value is the sum of the hydrogen mass and one third of electron mass. Similarly, we took $m=3670.8162$ a.u. (which is the sum of the deuterium mass and one third of electron mass) for D_3^-.

The resulting adiabatic potentials of A_1' and A_2' irreps are shown in Fig. 6 for H_3^- and in Fig. 7 for D_3^-. The curves of E'
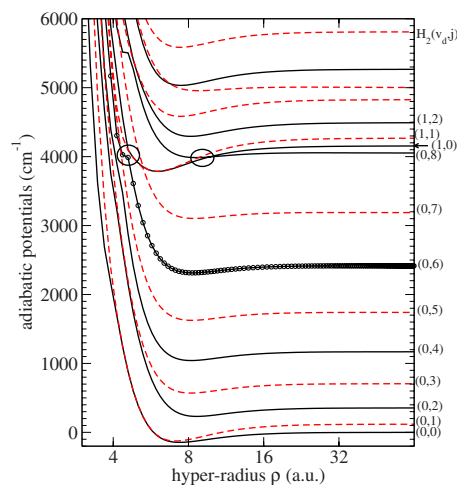

FIG. 6. The lowest H_3^- hyperspherical adiabatic curves [$U_a(\rho)$ in Eq. (13)] for $J=0$ of A_1' irrep (solid black lines) and of A_2' irrep (dashed red lines). The curves of the E' irrep are not displayed, as they are very similar to the A_1' and A_2' curves for energies smaller than 4000 cm^{-1} above the lowest dissociation limit $H_2(0,0)+H^-$, and would be indistinguishable on this scale. A couple of avoided crossings located around 4000 cm^{-1} are marked. Each curve is labeled at large R with the pair of indexes (v_d,j) corresponding to the rovibrational state of the H_2 molecule. The energy origin is set to the lowest dissociation limit $H_2(0,0)+H^-$. The closed circles on the $(0,6)$ curve exemplifies the density of grid points in R used in the calculations.

irrep are not shown in Figs. 6 and 7. The lowest E' curves are almost identical to the A_1' and A_2' curves and would be indistinguishable from them in the figures because for low vibrational levels, the energies of levels are independent on the symmetry (A_1', A_2', or E') of wave functions with respect to the proton exchange between the dimer and the H^- ion. (We assume here that the dimer is in a particular rovibrational state such that the proton exchange is made without changing the dimer state. The energy does depend on the H_2 rovibrational state). At large ρ, all adiabatic curves dissociate into an atom+dimer system characterized by the rovibrational state (v_d,j) of the dimer.

Some of the adiabatic curves in Figs. 6 and 7 exhibit avoided crossings at energies above $\sim$4000 cm^{-1}. Dynamic
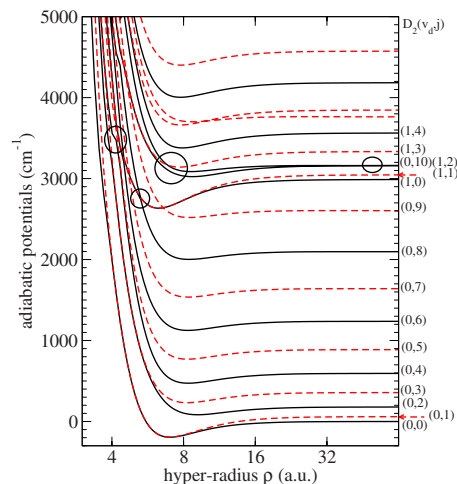

FIG. 7. Same as Fig. 6 for the D_3^- molecule. The energy origin here is set to the lowest dissociation limit $D_2(0,0)+D^-$. A few avoided crossings are indicated by circles.

TABLE II. Comparison of energies (in cm^{-1}) of H_3^- bound levels obtained in the present study with those of Ref. 10. Energies in the second and third columns are given with respect to D_{as} (see Table I). The binding energies (fourth and fifth columns) are given with respect to the dissociation limits D_{00} (for A_1' levels) and D_{01} (for A_2' levels). The energies in parentheses are given with respect to D_{00}, to compare with Ref. 10.

	Energies above D_{as}		Binding energies	
$J,\Omega,j,v_t,v_d,\Gamma$	Present study	Calculations of Ref. 10	Present study	Calculations of Ref. 10
$0,0,0,0,0,A_1'$	2103.3	2100.6	−70.7	−68.4
$0,0,0,1,0,A_1'$	2148.4	2147.1	−25.6	−21.9
$0,0,0,2,0,A_1'$	2168.7	2165.9	−5.4	−3.1
$0,0,0,3,0,A_1'$	2174.1	2168.7	−0.01	−0.3
D_{00} [a]	2174.1	2169.0		
$0,0,1,0,0,A_2'$	2140.3	2140.8	−152.1 (−33.7)	n/a (−28.2)
$0,0,1,1,0,A_2'$	2215.1		−77.4	
$0,0,1,2,0,A_2'$	2259.3		−33.2	
$0,0,1,3,0,A_2'$	2281.9		−10.6	
$0,0,1,4,0,A_2'$	2290.9		−1.6	
D_{01} [b]	2292.5	n/a		

[a]Asymptotic energy of $H^-+H_2(v_d=0,j=0)$ dissociation.
[b]Asymptotic energy of $H^-+H_2(v_d=0,j=1)$ dissociation.

coupling between hyperspherical adiabatic states is mostly determined by the avoided crossings and responsible for nuclei exchange above the potential barrier identified in Fig. 2. Such transitions are much less probable at smaller energies as each adiabatic state is only weakly coupled to other adiabatic states of the same irrep. As a consequence, only one component φ_a in the expansion of Eq. (11) is dominant. Each adiabatic state for a given irrep Γ is correlated with a definite pair of quantum numbers (v_d,j), and can be approximately characterized by these two quantum numbers. The value Ω of the projection of the H_2 angular momentum $\mathbf{j}$ on the axis connecting the dimer with the atom is also a relevant quantum number. For $J=0$, Ω is always zero and, therefore is not specified in Figs. 6 and 7.

To characterize completely a bound state of the trimer, an additional quantum number v_t is needed for the excitation within each adiabatic state (along the hyper-radius). Therefore, the bound states are characterized by four approximate quantum numbers Ω,j,v_t,v_d and two exact quantum numbers J and Γ. At high energies, the mixing between different Ω,j,v_t,v_d for given J and Γ becomes important.

We summarized in Table II the present H_3^- bound state energies and those of Ref. 10 labeled with the set of quantum numbers $J,j,\Omega,v_t,v_d,\Gamma$. In agreement with Ref. 10, we found four vibrational energies levels of the A_1' irrep and one other level of the A_2' irrep. We also found four more vibrational levels of the A_2' irrep. Although their energies are located above the $v_d=0,j=0$ dissociation threshold, they are stable because they cannot dissociate due to the symmetry restriction. Their binding energies are given in the table with respect to their first allowed dissociation limit $v_d=0,j=1$. It is worth noticing that our binding energies for all levels but one are larger than the energies of Ref. 10, expressing that the well depth of our potential surface is found about 17 cm^{-1} deeper than in Ref. 10). The last bound level of the A_1' irrep has a very small binding energy and may not be

TABLE III. Energies (in cm^{-1}) of D_3^- bound levels obtained in the present study. Energies in the second column are given with respect to D_{as} (see Table I, D_{as} being the same for H_3^- and D_3^-). The binding energies in the third column are given with respect to the dissociation limits D_{00} for the A_1' levels and D_{01} for the A_2' levels. The D_{00} and D_{01} dissociation D_2+D^- limits are calculated with respect to D_{as} and also given in the table.

$J,\Omega,j,v_t,v_d,\Gamma$	Energies above D_{as}	Binding energies
$0,0,0,0,0,A_1'$	1416.5	−126.2
$0,0,0,1,0,A_1'$	1474.1	−68.6
$0,0,0,2,0,A_1'$	1510.1	−32.6
$0,0,0,3,0,A_1'$	1530.2	−12.5
$0,0,0,4,0,A_1'$	1539.8	−2.9
$0,0,0,5,0,A_1'$	1542.7	−0.02
D_{00} [a]	1542.7	
$0,0,1,0,0,A_2'$	1419.9	−182.3
$0,0,1,1,0,A_2'$	1485.0	−117.2
$0,0,1,2,0,A_2'$	1532.0	−70.3
$0,0,1,3,0,A_2'$	1563.8	−38.5
$0,0,1,4,0,A_2'$	1583.7	−18.7
$0,0,1,5,0,A_2'$	1595.1	−7.2
$0,0,1,6,0,A_2'$	1600.6	−1.7
$0,0,1,7,0,A_2'$	1602.3	−0.01
D_{01} [b]	1602.3	

[a]Asymptotic energy of $D^-+D_2(v_d=0,j=0)$ dissociation.
[b]Asymptotic energy of $D^-+D_2(v_d=0,j=1)$ dissociation.

fully converged. The bound state energies of D_3^- are given in Table III. Since the D_3^- molecule is heavier than H_3^-, it has more vibrational levels. No data from previous calculation is available for D_3^-.

In Appendix, Sec. 2, we estimate also the role of diagonal non-Born–Oppenheimer couplings, which is found to be smaller or comparable to the accuracy of the present calculations.

V. PERMANENT DIPOLE MOMENT SURFACE FOR THE H_3^- GROUND STATE

For calculation of different observables (such as the RA cross section) involving matrix elements of the dipole moment, the components of the permanent dipole moment for each geometry should be evaluated. In contrast with neutral charge distributions, the magnitude of the dipole moment vector for charged species depends on the origin of the coordinates. The dipole moment approximation for electromagnetic transitions requires a vector computed with the origin at the center of mass of the system.

The MOLPRO package delivers also the components of the permanent dipole moment together with the PES. For a fixed geometry, the obtained components of the dipole moment correspond to the coordinate system with the X,Y,Z axes along the principal axes of inertia of the molecule with the origin at the center of mass of the system. In our notations, the Y-axis is orthogonal to the plane of H_3^-, therefore $D_Y=0$. For $\gamma=0°$ and $90°$ there is only one non-zero component (D_Z in our notations). D_Z becomes also equal to zero at equilateral geometries. For other geometries ($\gamma \neq 0°$ or $90°$) there are two nonzero components, D_Z and D_X. We used the following convention to label the components: at large values of R, the component D_Z is the largest of the two in
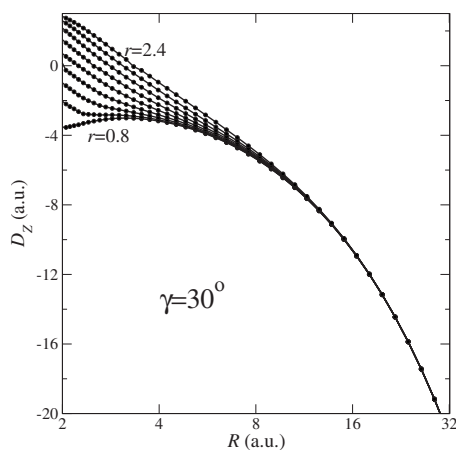
FIG. 8. The figure shows the D_Z component of the permanent electric dipole of H_3^- for one value of $\gamma = 30°$ and several values of r from $r = 0.8$ (the largest value of D_Z at small R) to 2.4 (the smallest value of D_Z at small R). The *ab initio* values and grid points are indicated by circles.

magnitude and negative, D_X being the smallest (in magnitude) and positive. The choice of negative D_Z at large R corresponds to the Z-axis oriented from the center of mass of the molecule toward the H^- ion. For small values of R (for fixed γ and r) the two components D_Z and D_X become comparable in magnitude. For such geometries they are identified by ensuring a smooth variation of the components with decreasing R. Notice that because the principal axes of inertia for H_3^- and D_3^- are the same, the obtained PDMS are the same for the two species.

Figures 8 and 9 show *ab initio* values of the D_Z and D_X PDM components for $\gamma = 30°$ for all nine values of $r = 0.8, 1, \cdots, 2.4$ a.u. as a function of R. As one can see from the figures, the sampling grid of *ab initio* geometries is dense enough to perform an interpolation procedure in order to calculate D_Z and D_X at any arbitrary geometry. Therefore, in the central region in Fig. 1, we interpolate the D_Z and D_X PDMS using the same 3D B-spline procedure as for the PES interpolation.

In region II, when $R \to \infty$, the analytical behavior of the largest component D_Z is known: It decreases with increasing
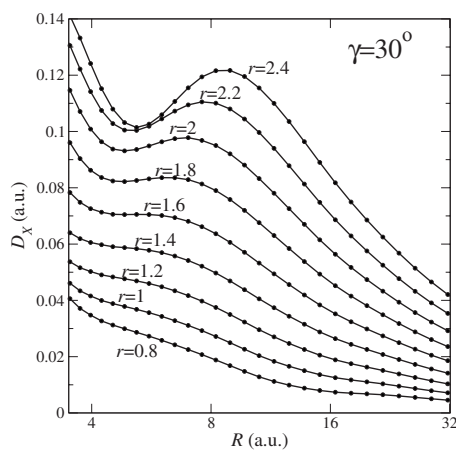

FIG. 9. The D_X component of the permanent dipole of H_3^- for $\gamma = 30°$ and different r. The *ab initio* values and grid points are indicated by circles.

R as (in a.u.) $D_Z \equiv e r_{\text{cm-H}} = -2R/3$, where $r_{\text{cm-H}}$ is the distance between the center of mass of H_3^- and the H^- ion, and $e \equiv -1$ is the electron charge. The *ab initio* D_Z values confirm this behavior, so the same formula is used for extrapolation of D_Z in region II. Outside the central region in Fig. 1, the PDMS (except the D_Z components in region II) are extrapolated using an empirical analytical formula. The empirical formula is obtained by inspecting the PDMS variations close to the boundaries of the *ab initio* region. The smallest component D_X varies at large R as $k_x(r, \gamma)/R$, where $k_x(r, \gamma)$ is fixed by the value of the PDMS at the final point $R_f = 56.4227$ a.u. of the grid, i.e., $k_x = V(R_f; r, \gamma) R_f$. As previously, we obtain a surface for the $k_x(r, \gamma)$ function, which is computed at any geometry using a 2D B-spline interpolation. For the extrapolation of the PDMS in region I we found (empirically) a quadratic (for D_Z) and linear (for D_X) dependencies along r with coefficients depending on R and γ, which are evaluated from the corresponding boundary values of D_Z and D_X, respectively. Similarly, in region III and IV, we assumed a linear dependency along r and R, respectively, with coefficients fixed by the boundary values of the PDMS.

VI. SUMMARY AND CONCLUSIONS

In the present study we have obtained accurate potential energy surface and components of the permanent dipole moment for the H_3^- molecular ion. The surfaces were calculated on a large number of geometries that covers short, intermediate, and long-range regions. In total, the *ab initio* calculations were made for 3024 geometries. The large basis and grid used in the calculations allows us to suggest that the obtained PES is more accurate than the results of the previous study.[10,11] Comparison of the long-range behavior of the obtained PES with the expected analytical behavior of the PES confirms this conclusion. No previous data on the dipole moment of H_3^- is available.

The obtained *ab initio* values for potential energy surface and the dipole moment components were used to construct FORTRAN interpolation/extrapolation subroutines that calculate the energies and dipole moments for any arbitrary geometry. The subroutines interpolate the surfaces using B splines inside the region of *ab initio* geometries and extrapolate the surfaces outside of the region using analytical formulas based on the theoretical asymptotic behavior. The subroutines are available in the supplementary material.[72] The energy surface can be used for all isotopologues of H_3^-, the dipole moment surfaces in the present form can only be used for H_3^- and D_3^- isotopologues. For the H_2D^- and D_2H^- molecules, the dipole moments should be transformed to account for the different orientation of axes of inertia. Using the new potential surfaces, we have calculated the bound states for the H_3^- and D_3^- isotopologues.

A relatively large magnitude $|D| \sim 4$ a.u. of the dipole moment near equilibrium positions for bound vibrational states and a large size of the electronic clouds of H^- suggest that the cross section for the formation of H_3^- stable molecules by the RA between H_2 and H^- is significant. A rela-

tively large dipole moment and the existence of several bound levels suggests also that the H$_3^-$ can be detected using IR photoabsorption spectroscopy.

The calculated energies of H$_3^-$ bound states can also be used to search for H$_3^-$ in the cold ISM with a large fraction of ionized hydrogen (to have enough free electrons). We have developed a model for the formation of H$_3^-$ in RA collisions between H$_2$ and H$^-$. In the model, H$^-$ is formed by dissociative attachment of the electron to H$_2$. If a photoabsorption signal from H$_3^-$ (in mm range) is detected, this would also be a signal for the presence of H$^-$ in the ISM: H$^-$ itself cannot be detected directly. The details of the model as well as the calculated rates of RA collisions between H$_2$ and H$^-$ will be discussed in a forthcoming publication.

ACKNOWLEDGMENTS

APPENDIX: ON THE ACCURACY OF THE PRESENT *AB INITIO* RESULTS

1. Comparison between MRCI and CEPA-2 methods

In this appendix, we discuss briefly the comparison of the results obtained using the CEPA-2 and multi reference configuration interaction (MRCI) *ab initio* methods. The CEPA method has been introduced about thirty years ago by Meyer and collaborators. Although the CEPA methods provide accurate results (at least, for certain molecules) and are not very expensive numerically (see, for instance, the recent review of Ref. 66), they have never been very popular in quantum chemistry calculations, even if a small part of the quantum chemistry community is still developing CEPA-type methods.[66–69]

To demonstrate the accuracy of the CEPA-2 method that has been employed for the present study, we have also performed calculations with the MRCI method using the same basis in the CEPA-2 calculation. In the MRCI calculations, all four electrons of H$_3^-$ are treated as active. We have used four active (self consistent field) orbitals. We have also verified that further increase of the number of active orbitals does not change the obtained energies for the geometries of interest. As pointed out above, at small distances near equilateral geometries the ion is unstable due to the electron autodetachment. Therefore, CEPA-2 and MRCI are not converging at such geometries with the employed basis.

The result of the comparison is given in Figs. 10 and 11. Figure 10 compares the *ab initio* energies of H$_3^-$ obtained using CEPA-2 and MRCI methods for fixed values of $\gamma=0$ and $r=1.4$ and different values of R. The figures includes also the results of MRCI calculations with Pople and Davidson corrections included (see Ref. 70 and references therein). The asymptotic limits of the four curves are quite different.
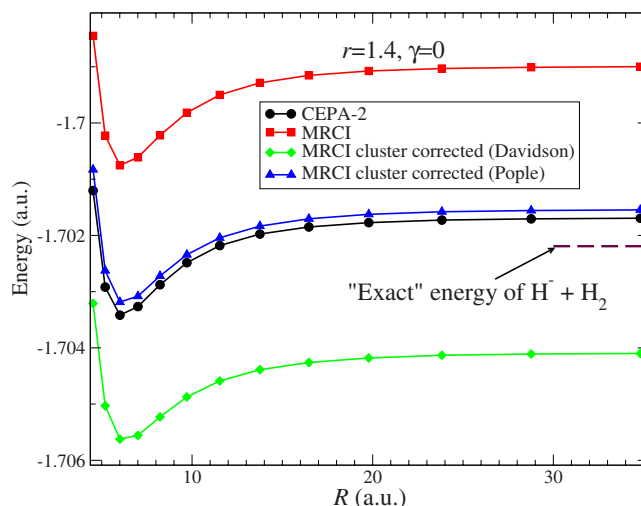

FIG. 10. Comparison of the results obtained using CEPA-2 and MRCI methods. The "exact" H$^-$+H$_2$ energy is obtained as the sum of the Born–Oppenheimer energy of the H$_2$ dimer for $r=1.4$ a.u. (Ref. 55), energy of H, 0.5 a.u., and the experimental affinity of H$^-$ (Ref. 56) (see Table I).

The CEPA-2 asymptotic energy is the closest one above the "best available" estimation 1.702 191 8 for the sum of H$_2$ and H$^-$ energy (see Table I). We recall that CEPA-2 method gives the energy of H$_3^-$ at $R \rightarrow \infty$ that is exactly equal to the sum of H$_2$ and H$^-$ energies calculated separately for H$_2$ and H$^-$ (see Table I). Based on this observation, we conclude that CEPA-2 provides better results than the corrected or uncorrected MRCI method.

Figure 11 shows the same curves as Fig. 10 but the asymptotic limits of the four curves are brought to the same value. As one can see the agreement between energies relative to the dissociation limit is much better than the agreement in terms of absolute energies. Notice that the potential well depth in Fig. 11 strongly depends on the correction added to the bare MRCI value, the latter being very close to the CEPA-2 one.
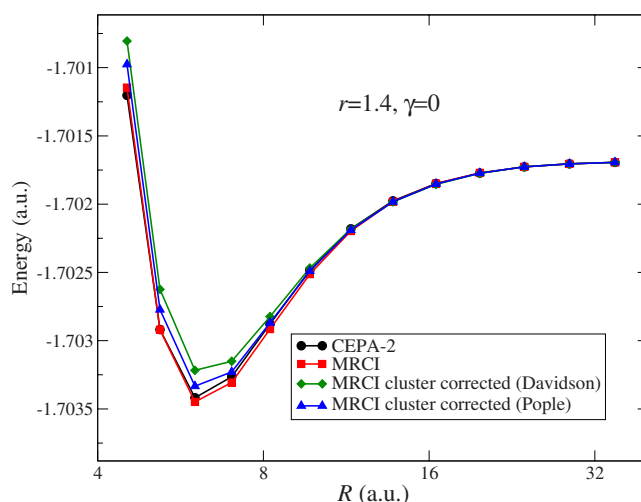

FIG. 11. CEPA-2 and MRCI energies relative to their dissociation limit for $r=1.4$ and $\gamma=0$. The four curves of Fig. 10 are brought to the same asymptotic limit by adding the corresponding energy. Notice that the R coordinate is shown in the logarithmic scale.

The remaining inaccuracy (≈ 100 cm^{-1} for CEPA-2) in the absolute energies should probably be attributed to the limited basis used in the present study.

2. On the diagonal non-Born–Oppenheimer correction

Here, we discuss the diagonal non-Born–Oppenheimer correction (DNBOC) to the obtained H$_3^-$ PES, which may be expected to have a significant contribution due to the low H$_3^-$ mass. As mentioned above, the H$_3^-$ molecule is a loosely bound H$_2$+H$^-$ complex. Therefore, for the estimation of DNBOC we can model it as the H$_2$ dimer with the internuclear distance r perturbed by the presence of H$^-$ located at the distance R with the angle γ. Therefore, the DNBO correction, $\epsilon(r, R, \gamma)$ can be represented as $\epsilon_0(r) + \epsilon_1(r, R, \gamma)$, where $\epsilon_0(r)$ is DNBOC of the dimer, and $\epsilon_1(r, R, \gamma)$ is the correction caused by the perturbation of the dimer due to the presence of H$^-$; $\epsilon_1(r, R, \gamma) \to 0$ when $R \to \infty$. We can estimate the order of magnitude of the $\epsilon_1(r, R, \gamma)$ term for geometries of the interest (near the minimum of H$_2$) as $\epsilon_1(r, R, \gamma)/\epsilon_0(r) \lesssim \Delta U(\text{H}_2)/U(\text{H}_2)$, where $\Delta U(\text{H}_2)$ is the change in H$_2$ energy due to the perturbation, i.e., the depth of the potential well of the H$_2$+H$^-$ complex, and $U(\text{H}_2)$ is the energy of the unperturbed H$_2$ dimer near the equilibrium. For $U(\text{H}_2)$ it is reasonable to take the energy of chemical bond of H$_2$, i.e., 0.174 475 7 a.u. Using these numbers we obtain $\epsilon_1(r, R, \gamma)/\epsilon_0(r) \lesssim 1/200$. The value $\epsilon_0(r=1.4)$ is about 100 cm^{-1},[55,71] which gives the estimation for $\epsilon_1(r, R, \gamma)$ of the order of 0.5 cm^{-1}. It is comparable to the accuracy of the present calculation (in terms of energies relative to the H$_2$+H$^-$ dissociation limit).

The function $\epsilon_0(r)$ is known[55,71] and can be added to the Born–Oppenheimer PES obtained in the present study. In calculation of bound states of H$_3^-$ we did not include DNBOC. For the all bound states of H$_3^-$ and D$_3^-$, the state of the dimer is the ground rovibrational level. Therefore, the binding energies shown in Tables II and III are insensitive to the inclusion of the correction. The inclusion of DNBOC is important if higher energies are involved, and especially when the H$_2$D$^-$ and D$_2$H$^-$ isotopologues are considered.

[1] A. Rau, J. Astrophys. Astron. **17**, 113 (1996).
[2] D. Stevenson and J. Hirschfelder, J. Chem. Phys. **5**, 933 (1937).
[3] J. T. Vanderslice and E. A. Mason, J. Chem. Phys. **33**, 492 (1960).
[4] C. Ritchie and H. King, J. Am. Chem. Soc. **90**, 825 (1968).
[5] A. Macías, J. Chem. Phys. **48**, 3464 (1968).
[6] A. Macías, J. Chem. Phys. **49**, 2198 (1968).
[7] G. Ramiro Garcia, A. R. Rossi, and A. Russek, J. Chem. Phys. **70**, 5463 (1979).
[8] G. Chalasinski, R. A. Kendall, and J. Simons, J. Phys. Chem. **91**, 6151 (1987).
[9] H. H. Michels and J. A. Montgomery, Chem. Phys. Lett. **139**, 535 (1987).
[10] J. Stärck and W. Meyer, Chem. Phys. **176**, 83 (1993).
[11] A. N. Panda and N. Sathyamurthy, J. Chem. Phys. **121**, 9343 (2004).
[12] R. E. Hurley, Nucl. Instrum. Methods **118**, 307 (1974).
[13] W. Aberth, R. Schnitzer, and M. Anbar, Phys. Rev. Lett. **34**, 1600 (1975).
[14] R. Schnitzer, R. W. Odom, and M. Anbar, J. Chem. Phys. **68**, 1489 (1978).
[15] Y. K. Bae, M. J. Coggiola, and J. R. Peterson, Phys. Rev. A **29**, 2888 (1984).
[16] W. Wang, A. K. Belyaev, Y. Xu, A. Zhu, C. Xiao, and X.-F. Yang, Chem. Phys. Lett. **377**, 512 (2003).
[17] R. Golser, H. Gnaser, W. Kutschera, A. Priller, P. Steier, A. Wallner, M. Čížek, J. Horáček, and W. Domcke, Phys. Rev. Lett. **94**, 223003 (2005).
[18] F. Robicheaux, Phys. Rev. A **60**, 1706 (1999).
[19] A. K. Belyaev and A. S. Tiukanov, Chem. Phys. **220**, 43 (1997).
[20] O. K. Kabbaj, F. Volatron, and J.-P. Malrieu, Chem. Phys. Lett. **147**, 353 (1988).
[21] A. K. Belyaev, D. T. Colbert, G. C. Groenenboom, and W. H. Miller, Chem. Phys. Lett. **209**, 309 (1993).
[22] A. K. Belyaev and A. S. Tiukanov, Chem. Phys. Lett. **302**, 65 (1999).
[23] A. K. Belyaev, A. S. Tiukanov, and W. Domcke, Phys. Rev. A **65**, 012508 (2001).
[24] A. K. Belyaev, A. S. Tiukanov, and W. Domcke, Phys. Scr. **80**, 048124 (2009).
[25] Here we use the traditional expression "non-Born–Oppenheimer" (non-BO) couplings to label the radial couplings between different electronic states. We keep the name "nonadiabatic couplings" for the couplings between the hyperspherical states of Sec. IV.
[26] J. E. E. Muschlitz, T. L. Bailey, and J. H. Simons, J. Chem. Phys. **24**, 1202 (1956).
[27] J. E. E. Muschlitz, T. L. Bailey, and J. H. Simons, J. Chem. Phys. **26**, 711 (1957).
[28] M. S. Huq, L. D. Doverspike, and R. L. Champion, Phys. Rev. A **27**, 2831 (1983).
[29] M. Zimmer and F. Linder, Chem. Phys. Lett. **195**, 153 (1992).
[30] M. Zimmer and F. Linder, J. Phys. B **28**, 2671 (1995).
[31] H. Müller, Z. Zimmer, and F. Linder, J. Phys. B **29**, 4165 (1996).
[32] E. Haufler, S. Schlemmer, and D. Gerlich, J. Phys. Chem. **101**, 6441 (1997).
[33] Y. Okumura, Y. Fujiwara, M. Kashiwagi, T. Kitagawa, K. Miyamoto, T. Morishita, M. Hanada, T. Takayanagi, M. Taniguchi, and K. Watanabe, Rev. Sci. Instrum. **71**, 1219 (2000).
[34] L. R. Grisham, M. Kuriyama, M. Kawai, T. Itoh, and N. Umeda, AIP Conf. Proc. **576**, 759 (2001).
[35] E. A. Mason and J. T. Vanderslice, J. Chem. Phys. **28**, 1070 (1958).
[36] S. Mahapatra, N. Sathyamurthy, S. Kumar, and F. A. Gianturco, Chem. Phys. Lett. **241**, 223 (1995).
[37] S. Mahapatra and N. Sathyamurthy, J. Phys. Chem. **100**, 2759 (1996).
[38] F. A. Gianturco and S. Kumar, J. Chem. Phys. **103**, 2940 (1995).
[39] W. Haque Ansari and N. Sathyamurthy, Chem. Phys. Lett. **289**, 487 (1998).
[40] A. K. Belyaev and A. S. Tyukanov, Chem. Phys. Rep. **18**, 1289 (2000).
[41] S. Mahapatra, Phys. Chem. Chem. Phys. **2**, 671 (2000).
[42] R. Jaquet and M. Heinen, J. Phys. Chem. A **105**, 2738 (2001).
[43] A. N. Panda, K. Giri, and N. Sathyamurthy, J. Phys. Chem. A **109**, 2057 (2005).
[44] K. Giri and N. Sathyamurthy, J. Phys. B **39**, 4123 (2006).
[45] L. Yao, L. Ju, T. Chu, and K.-L. Han, Phys. Rev. A **74**, 062715 (2006).
[46] K. Giri and N. Sathyamurthy, Chem. Phys. Lett. **444**, 23 (2007).
[47] F. Aguillon, A. K. Belyaev, V. Sidis, and M. Sizun, Phys. Chem. Chem. Phys. **2**, 3577 (2000).
[48] T. Takayanagi and Y. Kurosaki, Phys. Chem. Chem. Phys. **2**, 665 (2000).
[49] V. Kokoouline, M. Ayouz, R. Guérout, M. Raoult, J. Robert, and O. Dulieu, e-print arXiv:0910.2330v1.
[50] W. Meyer, J. Chem. Phys. **58**, 1017 (1973).
[51] MOLPRO, a package of ab initio programs designed by H.-J. Werner and P. J. Knowles, version 2008.3, R. D. Amos, A. Bernhardsson, A. Berning *et al.*
[52] A. D. Buckingham, Adv. Chem. Phys. **12**, 107 (1967).
[53] J. D. Poll and L. Wolniewicz, J. Chem. Phys. **68**, 3053 (1978).
[54] W. Kołos and L. Wolniewicz, J. Chem. Phys. **46**, 1426 (1967).
[55] L. Wolniewicz, J. Chem. Phys. **99**, 1851 (1993).
[56] K. R. Lykke, K. K. Murray, and W. C. Lineberger, Phys. Rev. A **43**, 6104 (1991).
[57] B. Johnson, J. Chem. Phys. **73**, 5051 (1980).
[58] O. I. Tolstikhin, S. Watanabe, and M. Matsuzawa, J. Phys. B **29**, L389 (1996).
[59] V. Kokoouline and F. Masnou-Seeuws, Phys. Rev. A **73**, 012702 (2006).
[60] J. Blandon, V. Kokoouline, and F. Masnou-Seeuws, Phys. Rev. A **75**, 042508 (2007).
[61] F. T. Smith, Phys. Rev. **120**, 1058 (1960).
[62] B. R. Johnson, J. Chem. Phys. **79**, 1916 (1983).
[63] V. Kokoouline, O. Dulieu, R. Kosloff, and F. Masnou-Seeuws, J. Chem. Phys. **110**, 9865 (1999).
[64] V. Kokoouline, O. Dulieu, R. Kosloff, and F. Masnou-Seeuws, Phys. Rev.

A **62**, 032716 (2000).

[65] P. R. Bunker and P. Jensen, *Molecular Symmetry and Spectroscopy* (NRC Research, Ottawa, 1998).

[66] F. Neese, A. Hansen, F. Wennmohs, and S. Grimme, Acc. Chem. Res. **42**, 641 (2009).

[67] F. Neese, F. Wennmohs, and A. Hansen, J. Chem. Phys. **130**, 144108 (2009).

[68] F. Wennmohs and F. Neese, Chem. Phys. **343**, 217 (2008).

[69] M. Nooijen and R. J. Le Roy, J. Mol. Struct.: THEOCHEM **768**, 25 (2006).

[70] W. Duch and G. H. F. Diercksen, J. Chem. Phys. **101**, 3018 (1994).

[71] W. Kołos and L. Wolniewicz, J. Chem. Phys. **41**, 3663 (1964).

[72] See supplementary material at http://dx.doi.org/10.1063/1.3424847 for PES and PDMS FORTRAN subroutines.